Lithuanian Journal of Physics, Vol. **60**, No. 1, pp. 78–89 (2020)

HYBRID ORGANIC-INORGANIC $Fe_3O(TFBDC)_3(H_2O)_3\cdot(DMF)_3$ COMPOUND SYNTHESIZED BY SLOW EVAPORATION METHOD: CHARACTERIZATION AND COMPARISON OF MAGNETIC PROPERTIES

A. Laurikėnas [a], K. Mažeika [b], D. Baltrūnas [b], R. Skaudžius [a], A. Beganskienė [a], and A. Kareiva [a]

[a] *Institute of Chemistry, Vilnius University, Naugarduko 24, 03225 Vilnius, Lithuania*
[b] *Center for Physical Sciences and Technology, Savanorių 231, 02300 Vilnius, Lithuania*
Email: aivaras.kareiva@chgf.vu.lt

Received 19 October 2019; revised 26 October 2019; accepted 4 November 2019

In this study for the synthesis of a hybrid organic-inorganic $Fe_3O(TFBDC)_3(H_2O)_3\cdot(DMF)_3$ compound a slow evaporation method has been suggested. The synthesis product was characterized using X-ray powder diffraction (XRD) analysis, scanning electron microscopy (SEM) and energy-dispersive X-ray spectroscopy (EDX) coupled with SEM and electron paramagnetic resonance (EPR) spectroscopy. The antiferromagnetic/weakly ferromagnetic behaviour of the synthesized sample was confirmed by magnetization measurements and Mössbauer spectroscopy. The synthesized magnetic material could be itself tested for different medical applications and could be used as precursor material for the preparation of nanostructured iron oxides with a variety of useful properties for biomedicine.

Keywords: hybrid materials, organic-inorganic, iron, slow evaporation method, magnetic properties

PACS: 75.50.–y, 75.60.Ej, 76.80.+y, 81.05.–t, 81.20–n

1. Introduction

The development of new materials or new synthesis routes for the materials applicable in medicine is still a big challenge [1–3]. Different compounds have been used in biotechnology and biomedicine for many years, however, the search for novel biomaterials to reach better quality of human life is the principal task for the scientists working in this area [4]. A number of different iron-containing compounds is widely used in the clinical applications, both in diagnostics and therapy. For example, recently Fe^{3+}-based polypeptides were suggested to use in diagnostic radiology instead of commercially available Gd containing magnetic resonance imaging (MRI) contrast reagents [5]. The magnetic resonance angiography studies showed an effective MRI contrast enhancement of the suggested compound. Iron-containing compounds could be used not only as contrast media for MRI, but also for drug delivery and targeting, as agents for hyperthermia and nanocarriers.

In the area of MRI, the Fe_3O_4 nanoparticles are widely used as contrast agents [6–10]. The combined method, based on susceptibility weighted images, has been developed to investigate human brains, particularly neural stem cells labelled with iron oxide. This method could be successfully

used in the diagnostics of ischemic disease. Moreover, the iron oxide nanoparticles modified with polymer could be used for the investigation of different microstructural features, also for drug delivery and, consequently, for theranostic purposes. Antibody-conjugated superparamagnetic nanoparticles could be applied for the measurement of the effects of drug treatments for Alzheimer's disease [9].

The hybrid organic-inorganic compounds containing lanthanides or iron were investigated as drug delivery systems and for specific tumour imaging [11, 12]. Even a simple coordination compound of iron shows potential application in specific diagnostics [13]. For the detection of accumulated metals or metal-containing compounds remaining after imaging in the brain tissues the high sensitive methods have been recently developed [14]. Superparamagnetic magnetite nanoparticles were functionalized with the natural anticoagulant, heparin [15–17]. The modified nanoparticles with heparin were successfully applied to prevent thrombosis and for cancer theranostics. The systems composed of the cancer drug, Doxorubicin, pH sensitive polymer and magnetic materials were developed for the transportation of drugs and targeted loading [18]. Importantly, these systems could be also used for drug delivery not only to the soft tissue but also to the bone. It is well known that osteonecrosis is a severe complication of high-dose corticosteroid therapy in cancer sick patients. Therefore, the effective imaging to detect transplanted bone marrow cells in osteonecrosis is very important. For this purpose, the injected ferumoxytol (type of iron) was also investigated [19].

However, the use of new different compounds in diagnostics and therapy should be done with care. For example, the analysis results of different parts of human body which were injected with theranostic compounds demonstrated the increased iron concentration in the liver and the bone [20]. The authors state that this hyper-amount of iron could cause a risk for liver fibrosis and cancer. Of course, the toxicity of metals is very dependent on their physicochemical form. Multi-functional magnetic nanovehicles for targeted and on-demand delivery of therapeutic molecules and imaging of defined tissues and organs are greatly important in personalized medicine for the precise early diagnosis, efficient prevention and therapy without toxicity. However, despite many years of research, there are still no such transport systems available.

Recently, we suggested several important luminescence materials which could be used for biomedical applications [21–23]. However, the development of new magnetic materials for possible magnetically-guided transport systems for delivery of drugs and genes has a great potential. These magnetic materials are still sought also for applications in magnetic resonance imaging, cancer therapy, bone and dental repair, tissue engineering, biosensors, and in many other aspects. In this study, the hybrid organic-inorganic compound of Fe^{3+} with 2,3,5,6-tetrafluoro-1,4-benzenedicarboxylic acid (TFBDC ligand) has been synthesized by a slow evaporation method [24] and investigated. For the characterization of magnetic properties of the synthesized compound, magnetization measurements and Mossbauer spectroscopy have been performed.

2. Experiment

Iron (III) acetate was synthesized from metallic iron powder by reacting it with glacial acetic acid/hydrogen peroxide [25]. The obtained product was purified by recrystallization from 2-isopropanol and was used as starting material in the slow evaporation synthesis. 2,3,5,6-tetrafluoro-1,4-benzenedicarboxylic acid (TFBDC), triethylamine, *N,N*-dimethylformamide, methanol and all other chemicals were purchased from *Merck* and *Sigma Aldrich*.

Triethylamine was diffused into a solution of 2,3,5,6-tetrafluoroterephthalic acid (0.04 g, 0.15 mmol) and iron (III) acetate (0.125 g, 0.15 mmol) in an ethanol/N,N-dimethylformamide (DMF) (1:1 v/v) mixture. The solution was kept in a 10 ml glass vial covered with a plastic cap. One hole was punctured in the plastic cap for slower diffusion. The atmosphere of triethylamine was created by placing a beaker with triethylamine in a desiccator. The vial was kept in the desiccator for 2 weeks. The precipitated red powders of $Fe_3O(TFBDC)_3(H_2O)_3{\cdot}(DMF)_3$ were filtered and washed with DMF (3 × 5 ml) and hexane (3 × 5 ml). The precipitate was slightly soluble in water, but stable in organic solvents. A schematic diagram of the synthesis is presented in Fig. 1.

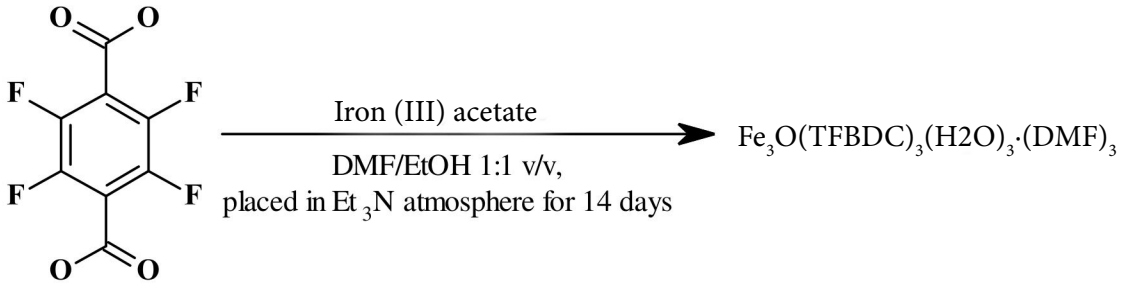

Fig. 1. Scheme of the synthesis of $Fe_3O(TFBDC)_3(H_2O)_3\cdot(DMF)_3$ by a slow evaporation method.

X-ray powder diffraction (XRD) analysis was performed in a region of $2\theta = 10–55°$ on a *Rigaku* Miniflex II diffractometer using Cu $K\alpha_1$ radiation with graphite filters. The XRD data were analysed on the Match 3 (*Crystal Impact*) software. The morphological characterization of the sample was carried out on a *Hitachi* TM3000 scanning electron microscope (SEM). Continuous-wave (CW) EPR measurements were performed at X-band microwave frequency (~9.4 GHz) using a conventional *Bruker* ELEXSYS E580 EPR spectrometer. A vibrating sample magnetometer consisting of a lock-in amplifier SR510 (*Stanford Research Systems*, USA), a gauss/teslameter FH-54 (*Magnet Physics*) and a laboratory magnet supplied by a power source SM 330-AR-22 (*Delta Elektronika*, Netherlands) was applied for the magnetization measurements. The magnetic susceptibility behaviour of the synthesized samples was studied with a SQUID magnetometer (*Quantum Design*, MPMS) at 300 K using the static field. The Mössbauer spectra were recorded with a Mössbauer spectrometer (*Wissenschaftliche Electronik GmbH*) from 11 K to room temperature using a source of ^{57}Co in the rhodium matrix.

3. Results and discussion

The phase crystallinity and purity of the synthesized hybrid organic-inorganic compound was characterized by means of X-ray diffraction analysis. The powder XRD pattern of the synthesized $Fe_3O(TFBDC)_3(H_2O)_3\cdot(DMF)_3$ is given in Fig. 2. The qualitatively recorded XRD pattern is comparable to the XRD patterns of similar lanthanide-containing hybrid compounds [22]. A high background observed in the XRD pattern of the synthesized compound indicates, probably, the formation of a partially amorphous phase or that the crystallization is very poor. These results are quite different from those published in [26] when a similar compound has been synthesized by using a perfluorinated linear dicarboxylate ligand. The strong absorption of X-rays by iron containing hybrid material was also observed. The correct crystal structure and phase information would be very important to understand the properties of this material, however, the identification of reflections in the XRD patterns was problematic, and therefore the crystal structure was not solved. On the other hand, no reflections attributable to other known iron crystalline phase were determined in the XRD pattern of the synthesized compound.

The SEM micrograph of the synthesized organic-inorganic hybrid material is shown in Fig. 3. Relatively large particles (15–20 μm) were formed during the slow evaporation method.

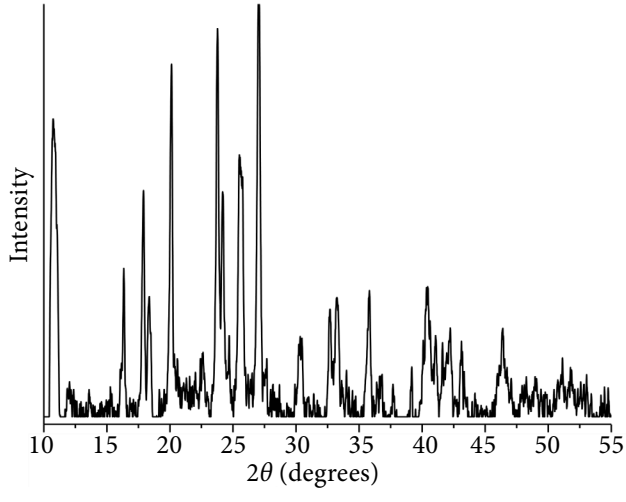

Fig. 2. XRD pattern of the synthesized $Fe_3O(TFBDC)_3(H_2O)_3\cdot(DMF)_3$.

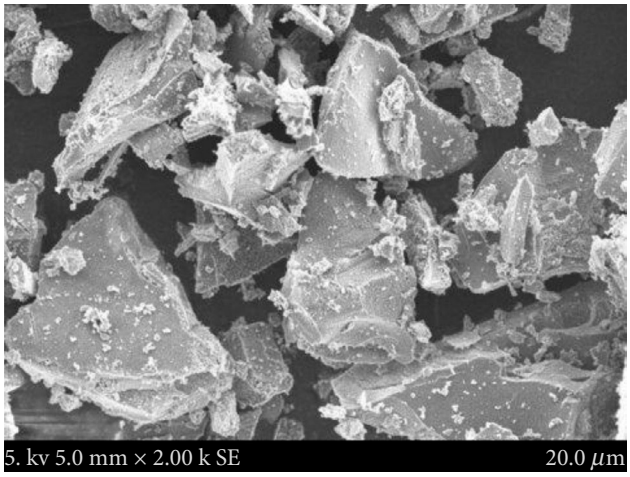

Fig. 3. SEM micrograph of the synthesized $Fe_3O(TFBDC)_3(H_2O)_3\cdot(DMF)_3$.

A similar size of the agglomerated particles was determined for the lanthanide-containing hybrid materials [22]. The most of these particles of $Fe_3O(TFBDC)_3(H_2O)_3\cdot(DMF)_3$ have a shape of a bulk triangle. These volumetric particles are slightly covered with differently shaped smaller particles. Energy-dispersive X-ray spectroscopy (EDX) was used for the determination of an elemental composition of the synthesized sample (see Table 1). The results presented in Table 1 show a good agreement between the experimentally determined and the calculated data indicating the possible correct composition $Fe_3O(TFBDC)_3(H_2O)_3\cdot(DMF)_3$ of the prepared hybrid material.

Table 1. Elemental analysis data for $C_{14}H_{27}O_{18}Fe_3$ determined by EDX.

Calculated, %	C 34.01; O 26.09; Fe 14.37; N 3.60; F 19.56
Determined, %	C 33.80; O 25.70; Fe 14.19; N 3.51; F 19.32

The electron paramagnetic resonance spectra of $Fe_3O(TFBDC)_3(H_2O)_3\cdot(DMF)_3$ obtained at different temperatures are shown in Fig. 4. The observed EPR lines at an electron g-factor of about 2 indicate the existence of Fe^{3+} (electron spin $S = 5/2$) [27]. The observed lines are very broad at both temperatures indicating strong spin-dipolar interactions between the paramagnetic Fe^{3+} ions [28, 29]. Strong exchange interactions between the electrons in the d orbitals of the Fe^{3+} ions might be responsible for line broadening as well [30].

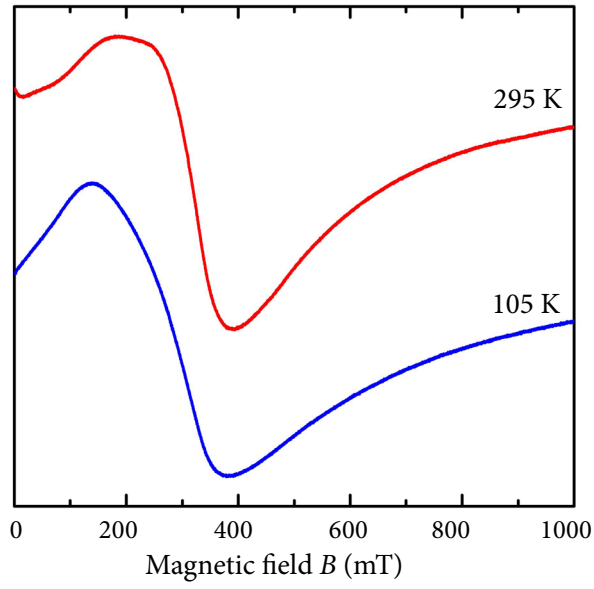

Fig. 4. Normalized EPR spectra of the synthesized $Fe_3O(TFBDC)_3(H_2O)_3\cdot(DMF)_3$ and recorded at 295 and 105 K.

It is well known that different properties of synthesized materials are very dependent on the used synthesis method [31]. Therefore, the magnetic properties of $Fe_3O(TFBDC)_3(H_2O)_3\cdot(DMF)_3$ synthesized by a slow evaporation method were studied in comparison with those of $Fe_3O(TFBDC)_3(H_2O)_3\cdot(DMF)_3$ synthesized by a precipitation method [22] and a similar $Fe_3O(BDC)_3(H_2O)_3\cdot(DMF)_3$ compound (here BDC is 1,4-benzendicarboxylic acid) obtained previously according to [32]. According to

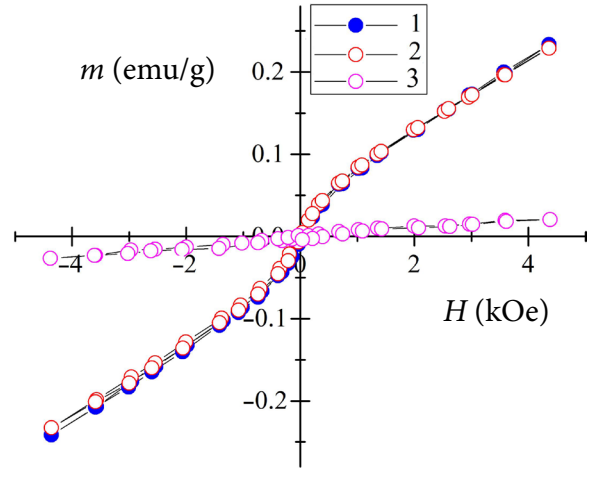

Fig. 5. The hysteresis loops for the differently synthesized $Fe_3O(TFBDC)_3(H_2O)_3\cdot(DMF)_3$ (1 for a precipitation method and 2 for a slow evaporation method) and $Fe_3O(BDC)_3(H_2O)_3\cdot(DMF)_3$ (3) hybrid compounds.

the magnetization measurements (Fig. 5), the iron-containing hybrid compounds with different ligands $Fe_3O(BDC)_3(H_2O)_3\cdot(DMF)_3$ and $Fe_3O(TFBDC)_3(H_2O)_3\cdot(DMF)_3$ show a different magnetic behaviour. The results of the magnetization measurements recorded for the differently synthesized $Fe_3O(TFBDC)_3(H_2O)_3\cdot(DMF)_3$ compounds coincide very well. Interestingly, the hysteresis of the $Fe_3O(BDC)_3(H_2O)_3\cdot(DMF)_3$ sample differs considerably from the sample with the TFBDC ligand. The paramagnetic behaviour of Fe(III) gives a linear dependence of magnetization on the strength of the magnetic field for the paramagnetic $Fe_3O(BDC)_3(H_2O)_3\cdot(DMF)_3$ sample according to Mössbauer spectroscopy (Figs. 5, 6). Evidently, the magnetization for the $Fe_3O(TFBDC)_3(H_2O)_3\cdot(DMF)_3$ samples is higher. However, the magnetization is low compared with ferro- or ferrimagnetic compounds of iron [33] and is characteristic of antiferromagnetic iron oxides/oxyhydroxides – hematite and goethite, as determined by Mössbauer spectroscopy (Figs. 7, 8). Magnetization of the hematite (above Morin transition) and goethite nanoparticles is caused by a small canting angle between antiferromagnetic sublattice magnetizations, uncompensated magnetic moments in antiferromagnetic nanoparticles and disordering of surface spins [34, 35].

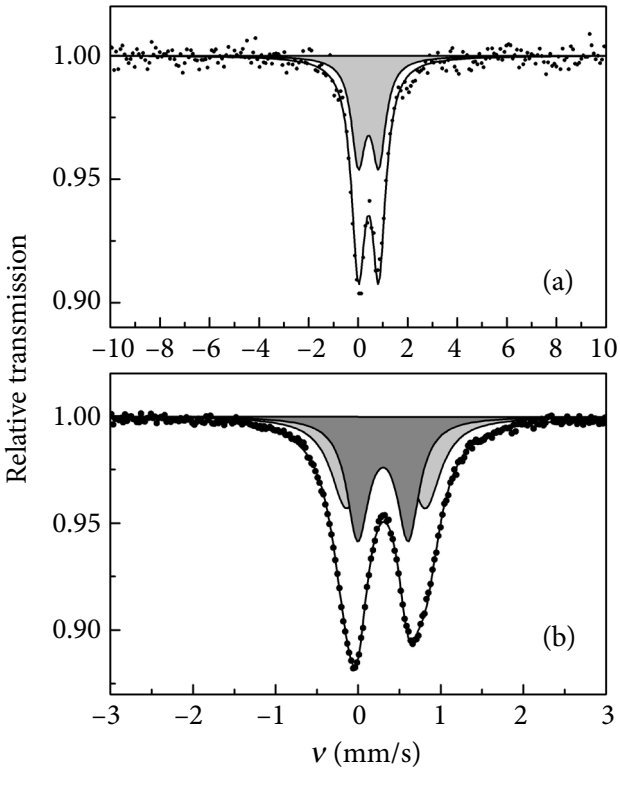

Fig. 6. Mössbauer spectra of the $Fe_3O(BDC)_3(H_2O)_3\cdot(DMF)_3$ sample at 11 K (a) and room temperature (b).

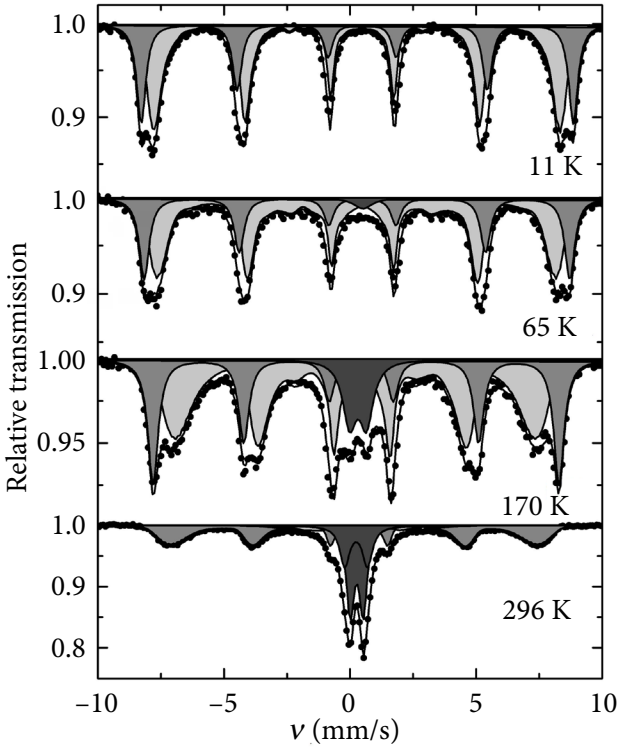

Fig. 7. Mössbauer spectra of the $Fe_3O(TFBDC)_3(H_2O)_3\cdot(DMF)_3$ sample at different temperatures.

The magnetization of the samples does not saturate at the applied magnetic fields because the canting angle and related uncompensated magnetic moment increase with magnetic field. For paramagnetic iron the magnetically split Mössbauer spectra can be observed only in diluted samples (<1 mol of Fe/L) [36]. For the $Fe_3O(TFBDC)_3(H_2O)_3\cdot(DMF)_3$ samples the area of Mössbauer spectra was fitted to the sextet and hyperfine field distribution at low temperature (Fig. 7). At T = 11 K hyperfine parameters of the sextet of the Fe1 site (35% of area) – hyperfine field $B \approx 53.11\pm0.03$ T, quadrupole shift $2\varepsilon = -0.197\pm0.004$ mm/s and isomer shift $\delta = 0.49\pm0.001$ mm/s – are such as for hematite [35]. The value of the quadrupole shift indicates hematite above the Morin transition temperature. For the bulk hematite Morin transition occurs at 263 K, but the temperature decreases for the nanocrystalline hematite and it is below 4 K when the size of hematite nanoparticles is smaller than 8–20 nm [35]. The rest of the spectrum at low temperature was fitted to the hyperfine field distribution which transforms to the doublet for

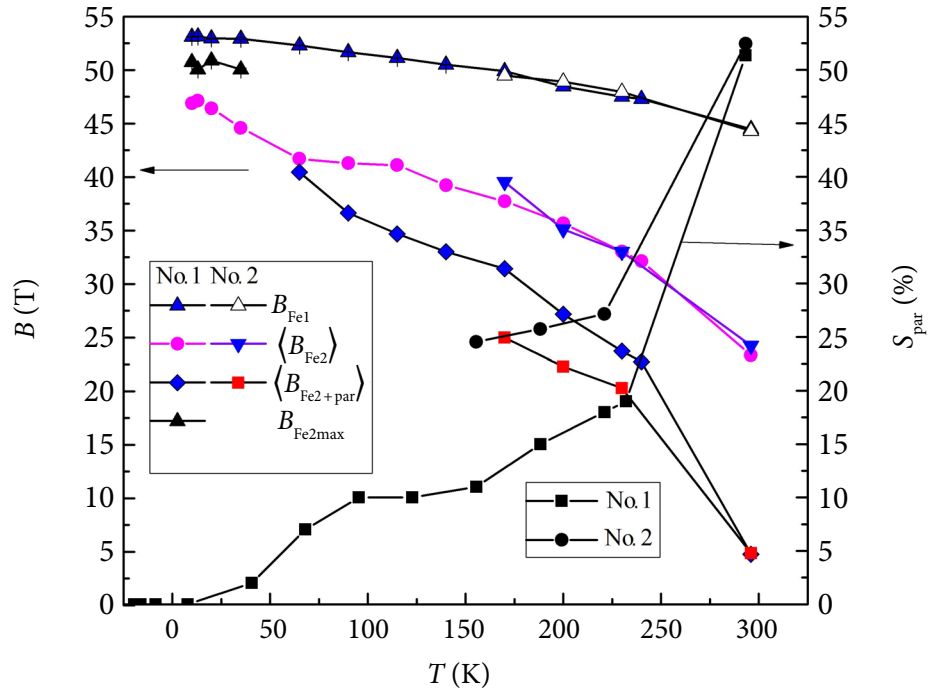

Fig. 8. Dependences of the hyperfine field of Fe1 and Fe2 sites (left) and percentage of the paramagnetic area of the Mössbauer spectrum (right) on temperature for the $Fe_3O(TFBDC)_3(H_2O)_3{\cdot}(DMF)_3$ synthesized by precipitation (No. 1) and slow evaporation (No. 2) methods.

the $Fe_3O(TFBDC)_3(H_2O)_3{\cdot}(DMF)_3$ samples when the temperature increases.

Though the quadrupole shift is similar for Fe1 and Fe2 iron structural sites, the values of the hyperfine field of Fe2 sites are distributed even at low temperature and are lower than that of the Fe1 site (Fig. 8). The most probable values of the hyperfine field and the quadrupole shift of the Fe2 site at low temperature are consistent with these parameters of goethite [37, 38]. At room temperature 35% of the area of the Mössbauer spectrum which is fitted using the hyperfine field distribution having the average value of the hyperfine field $\langle B \rangle \approx 44$ T (Fig. 8) is attributed to hematite nanoparticles. The doublets and another hyperfine field distribution (13% of area, $\langle B \rangle \approx 23$ T) are caused by goethite nanoparticles. The hyperfine field of ≈36 T characteristic of the well-crystallized goethite at room temperature decreases because of poor crystallinity and the influence of superparamagnetic relaxation38]. The change in the area of the paramagnetic part (samples No. 1 and No. 2) of Mössbauer spectra indicates the influence of the method of preparation on the size and crystallinity of Fe goethite nanoparticles.

The compound prepared from a precursor containing a different valency of iron in the molar ratio Fe(II):Fe(III) = 2:1, having the composition $Fe(II)_2Fe(III)O(TFBDC)_3(H_2O)_3{\cdot}(DMF)_3$, was also synthesized by a slow evaporation method. Surprisingly, for this sample the determined magnetization is the highest (Fig. 9). Two kinds of magnetic

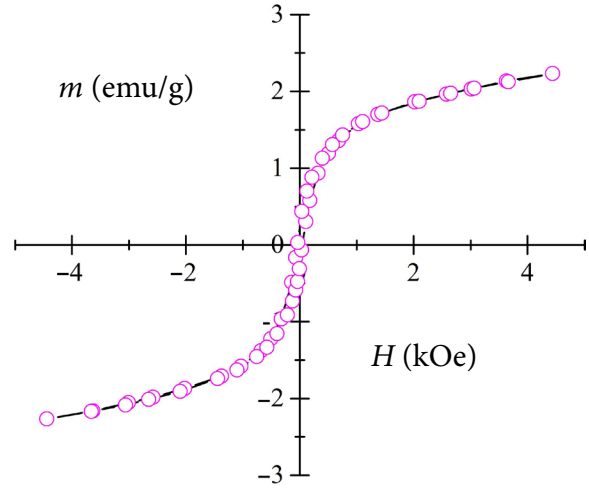

Fig. 9. The hysteresis loop for the $Fe(II)_2Fe(III)O(TFBDC)_3(H_2O)_3{\cdot}(DMF)_3$ compound.

ions in the precursor can result in the formation of ferrimagnetic ordering having unequal magnetic sublattices what leads to the increase of uncompensated magnetization. The Mössbauer data (Figs. 10, 11) indicate the presence of paramagnetic Fe(II) according to the parameters of the doublet having the quadrupole splitting Δ = 2.04±0.01 mm/s and the isomer shift δ = 1.32±0.01 mm/s at 11 K, and the area of which is about 7%. At low temperature (11–27 K) broad Mössbauer spectra of $Fe(II)_2Fe(III)O(TFBDC)_3(H_2O)_3\cdot(DMF)_3$ cannot be fitted to only one hyperfine field distribution (Fig. 10). A good fitting quality of the spectra is achieved using three hyperfine field distributions. Hyperfine field distributions covering 30, 20 and 43% of the area have almost equal average hyperfine fields ($\langle B \rangle \approx 44.6$, 46.4 and 45.65 T) but different quadrupole shifts (2ε = 0.43±0.02, –0.60±0.02 and –0.09±0.01 mm/s) at 11 K. The values of hyperfine fields are distributed up to approximately 55 T having the maximum probability at ≈48 T (Fig. 11). Akaganeite β-FeOOH stabilized by Cl or F ions has Fe sites characterized by different quadrupole shifts and hyperfine fields of 46.7–49.7 T [39] that are quite similar to the most probable hyperfine fields of the $Fe(II)_2Fe(III)O(TFBDC)_3(H_2O)_3\cdot(DMF)_3$ sample. In the case of chlorine stabilized β-FeOOH the transition temperature from an antiferromagnetic to a paramagnetic state is lower than room temperature (250–296 K) and depends on the amount of crystalline water [40]. Probably, a poor crystallinity of akaganeite obtained by hydrolysis of FeF_3 [39] results in the decrease of transition temperature to 200 K.

For the $Fe(II)_2Fe(III)O(TFBDC)_3(H_2O)_3\cdot(DMF)_3$ sample the transition temperature to a paramagnetic or a superparamagnetic state is considerably lower, between 30 K and room temperature, i.e. at 170 K more than 80% of material are in a paramagnetic/superparamagnetic state (Fig. 10). This can be explained by smaller sizes of the formed nanoparticles compared with these obtained at usual

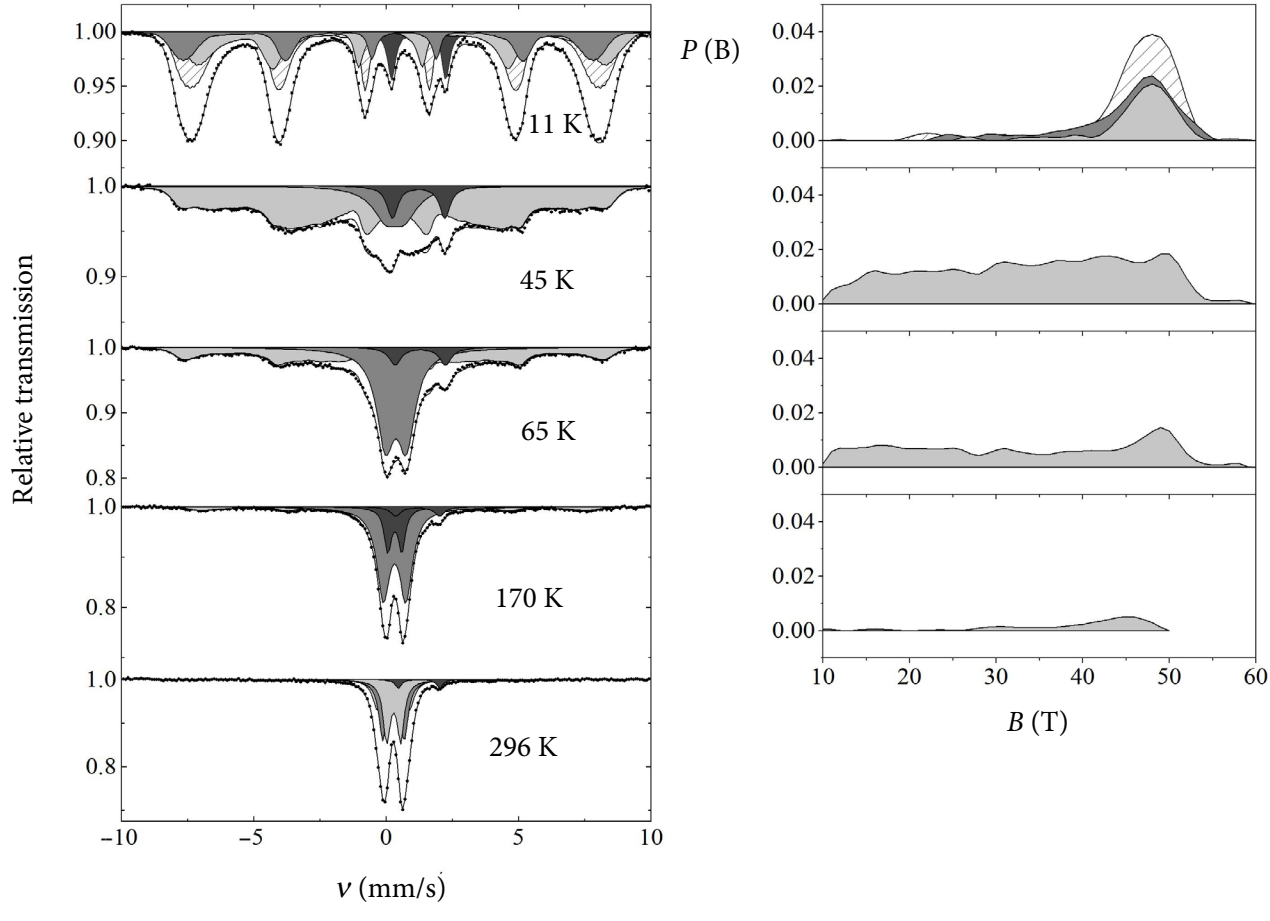

Fig. 10. Mössbauer spectra of the $Fe(II)_2Fe(III)O(TFBDC)_3(H_2O)_3\cdot(DMF)_3$ sample at different temperatures. Hyperfine field distributions fitted to the spectra are shown on the right.

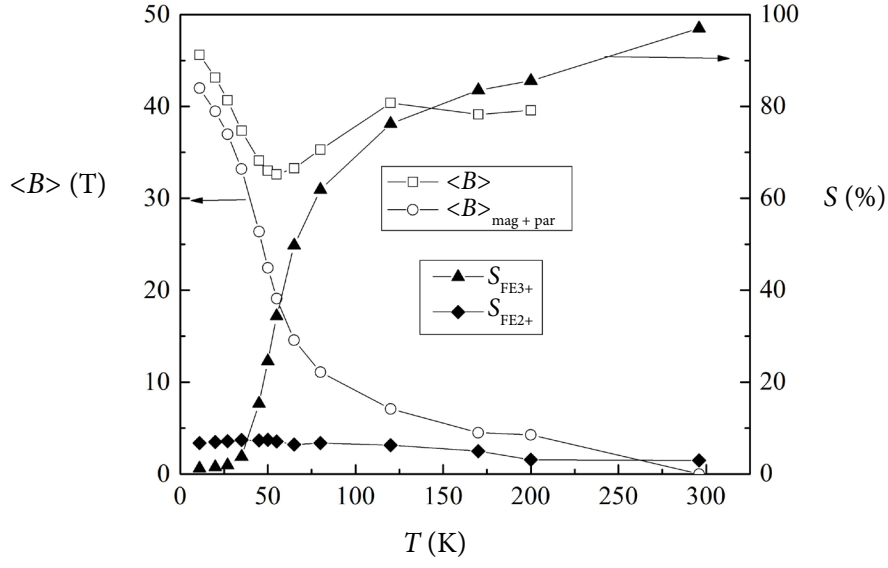

Fig. 11. Dependences of the average hyperfine field (left) and percentage of the paramagnetic area of the Mössbauer spectrum for Fe^{3+} and Fe^{2+} (right) on temperature for the $Fe(II)_2Fe(III)O(TFBDC)_3(H_2O)_3\cdot(DMF)_3$ sample.

conditions of akageneite preparation [39, 40]. Somatoid-type nanoparticles of a typical diameter of ≈25 nm and a length of ≈200 nm are characteristic of akaganeite obtained by hydrolysis [39]. An admixture of other Fe oxyhydroxides [41] is less likely. The observed magnetization (Fig. 9) is not compatible with the paramagnetic state of akaganeite β-FeOOH at room temperature. However, the β-FeOOH structural decay in reducing environments can form a ferrimagnetically ordered phase [42, 43]. Because of partial transformations the ferrimagnetic state may coexist with antiferromagnetic and quasi amorphous intermediate states depending on preparation conditions.

The synthesized new organic-inorganic hybrid material, taking into account its magnetic properties, could be itself tested for different medical applications, for example, for surface modification of implants to facilitate the integration process [44]. Moreover, this material could be successfully applied as a precursor for the synthesis of nanostructured iron oxides (wustite, hematite, maghemite, magnetite, goethite or different mixtures). Depending on the field of application, various magnetic properties are required. For instance, to fabricate wustite Fe_xO with homogeneous morphology and controlled phase composition and stoichiometry still is a challenging task [45]. Using such type of a precursor the synthesis of differently shaped nanostructures (spherical or ellipsoidal nanoparticles, nanowires, nanorods) and particles with different microstructure could be realized [45–47]. The mesoporous iron oxides and a variation of porosity of materials could also be achieved using the hybrid precursors with a prospective application in bionanotechnology [48]. The high quality nanoparticles as ferrofluids with enhanced magnetic properties could be also obtained and successfully used in biomedicine [49].

4. Conclusions

The hybrid organic-inorganic $Fe_3O(TFBDC)_3(H_2O)_3\cdot(DMF)_3$ compound was synthesized using a slow evaporation method. The XRD pattern of the synthesized hybrid material contained a high background indicating the formation of a partially amorphous phase. The obtained hybrid organic-inorganic products are composed of relatively large crystallites (15–20 μm); however, according to our previous studies, these crystallites could result from small particles via an agglomeration process. The observed EPR spectra at different temperatures were very broad indicating strong spin-dipolar interactions between the paramagnetic Fe^{3+} ions. The magnetization and Mössbauer data of the $Fe_3O(TFBDC)_3(H_2O)_3\cdot(DMF)_3$ sample considering the composition of the sample were

explained by superparamagnetism of the formed Fe oxide/hydroxide nanoparticles. The synthesized magnetic material could be itself tested for different medical applications and could be used as precursor material for the preparation of nanostructured iron oxides with a variety of useful properties for biomedicine. According to the magnetization measurements and Mössbauer spectroscopy data, the iron-containing hybrid $Fe_3O(BDC)_3(H_2O)_3 \cdot (DMF)_3$ compound was paramagnetic at any investigated temperature.

Acknowledgements

This work was supported by a Research Grant BUNACOMP (No. S-MIP-19-9) from the Research Council of Lithuania. The authors would like to thank Dr. Mantas Šimėnas for the EPR measurements.

References

[1] Y.Y. Lin and C.B. Mao, Bio-inspired supramolecular self-assembly towards soft nanomaterials, Front. Mater. Sci. **5**, 247–265 (2011).

[2] N. Fukuda, A. Tsuchiya, J. Sunarso, R. Toita, K. Tsuru, Y. Mori, and K. Ishikawa, Surface plasma treatment and phosphorylation enhance the biological performance of poly(ether ether ketone), Colloids Surf. B Biointerfaces **173**, 36–42 (2019).

[3] M. Abumanhal, R. Ben-Cnaan, I. Feldman, S. Keren, and I. Leibovitch, Polyester urethane implants for orbital trapdoor fracture repair in children, J. Oral Maxillofac. Surg. **77**, 126–131 (2019).

[4] H.J. Maeng, D.H. Kim, N.W. Kim, H. Ruh, D.K. Lee, and H. Yu, Synthesis of spherical Prussian blue with high surface area using acid etching, Curr. Appl. Phys. **18**, S21–S27 (2018).

[5] Y.D. Miao, F.N. Xie, J.Y. Cen, F. Zhou, X.F. Tao, J.F. Luo, G.C. Han, X.L. Kong, X.M. Yang, J.H. Sun, and J. Ling, Fe^{3+}@polyDOPA-*b*-polysarcosine, a T_1-weighted MRI contrast agent via controlled NTA polymerization, ACS Macro Lett. **7**, 693–698 (2018).

[6] R.T. Cha, J.J. Li, Y. Liu, Y.F. Zhang, Q. Xie, and M.M. Zhang, Fe_3O_4 nanoparticles modified by CD-containing star polymer for MRI and drug delivery, Colloids Surf. B Biointerfaces **158**, 213–221 (2017).

[7] D. Chelminiak, M. Ziegler-Borowska, and H. Kaczmarek, Polymer coated magnetite nanoparticles for biomedical applications. Part II. Fe_3O_4 nanoparticles coated by synthetic polymers, Polimery **60**, 87–94 (2015).

[8] J.R. Pinney, G. Melkus, A. Cerchiari, J. Hawkins, and T.A. Desai, Novel functionalization of discrete polymeric biomaterial microstructures for applications in imaging and three-dimensional manipulation, ACS Appl. Mater. Interfaces **6**, 14477–14485 (2014).

[9] M.A. Tafoya, S. Madi, and L.O. Sillerud, Superparamagnetic nanoparticle-enhanced MRI of Alzheimer's disease plaques and activated microglia in 3X transgenic mouse brains: Contrast optimization, J. Magn. Res. Imaging **46**, 574–588 (2017).

[10] Y. Kuwahara, T. Miyazaki, Y. Shirosaki, G.G. Liu, and M. Kawashita, Structures of organic additives modified magnetite nanoparticles, Ceram. Int. **42**, 6000–6004 (2016).

[11] H.H. Zou, L. Wang, C.H. Zeng, X.L. Gao, Q.Q. Wang, and S.L. Zhong, Rare-earth coordination polymer micro/nanomaterials: Preparation, properties and applications, Front. Mater. Sci. **12**, 327–347 (2018).

[12] S. Aryal, J. Key, C. Stigliano, J.S. Ananta, M. Zhong, and P. Decuzzi, Engineered magnetic hybrid nanoparticles with enhanced relaxivity for tumor imaging, Biomaterials **34**, 7725–7732 (2013).

[13] K. Roshani, M. Etemadzade, R. Farhoudi, S.E.S. Ebrahimi, M.P. Hamedani, A. Assadi, and M.S. Ardestani, Fe^{3+}-EDTA-zinc oxide nano-diagnostics: Synthesis and in vitro cellular evaluation, Biosci. Biotechnol. Res. Commun. **10**, 445–454 (2017).

[14] J.F. Collingwood and F. Adams, in: *Metals in the Brain: Measurement and Imaging*, Neuromethods, Vol. 124, ed. A.R. White (Humana Press, New York, 2017) pp. 7–32.

[15] S.C. Wuang, K.G. Neoh, E.-T. Kang, D.W. Pack, and D.E. Leckband, Heparinized magnetic

nanoparticles: In-vitro assessment for biomedical applications, Adv. Funct. Mater. **16**, 1723–1730 (2006).

[16] E. Vismara, A. Valerio, A. Coletti, G. Torri, S. Bertini, G. Eisele, R. Gornati, and G. Bernardini, Non-covalent synthesis of metal oxide nanoparticle-heparin hybrid systems: A new approach to bioactive nanoparticles, Int. J. Molec. Sci. **14**, 13463–13481 (2013).

[17] M.D. Rodriguez-Torres, L.S. Acosta-Torres, and L.A. Diaz-Torres, Heparin-based nanoparticles: An overview of their applications, J. Nanomater., Article ID 9780489 (2018).

[18] L.P. Wang, G. Jang, D.K. Ban, V. Sant, J. Seth, S. Kazmi, N. Patel, Q.Q. Yang, J. Lee, W. Janetanakit, S.S. Wang, B.P.vHead, G. Glinsky, and R. Lal, Multifunctional stimuli responsive polymer-gated iron and gold-embedded silica nano golf balls: Nanoshuttles for targeted on-demand theranostics, Bone Res. **5**, Article No. 17051 (2017).

[19] A.J. Theruvath, H. Nejadnik, A.M. Muehe, F. Gassert, N.J. Lacayo, S.B. Goodman, and H.E. Daldrup-Link, Tracking cell transplants in femoral osteonecrosis with magnetic resonance imaging: a proof-of-concept study in patients, Clinic. Cancer Res. **24**, 6223–6229 (2018).

[20] M. Regenboog, A.E. Bohte, E.M. Akkerman, J. Stoker, and C.E.M. Hollak, Iron storage in liver, bone marrow and splenic Gaucheroma reflects residual disease in type 1 Gaucher disease patients on treatment, British J. Haematol. **179**, 635–647 (2017).

[21] A. Prichodko, F. Enrichi, Z. Stankeviciute, A. Benedetti, I. Grigoraviciute-Puroniene, and A. Kareiva, Study of Eu^{3+} and Tm^{3+} substitution effects in sol-gel fabricated calcium hydroxyapatite, J. Sol-Gel Sci. Technol. **81**, 261–267 (2017).

[22] A. Laurikenas, A. Katelnikovas, R. Skaudzius, and A. Kareiva, Synthesis and characterization of Tb^{3+} and Eu^{3+} metal-organic frameworks with $TFBDC^{2-}$ linkers, Opt. Mater. **83**, 363–369 (2018).

[23] A. Smalenskaite, A.N. Salak, M.G.S. Ferreira, R. Skaudzius, and A. Kareiva, Sol-gel synthesis and characterization of hybrid inorganic-organic Tb(III)-terephthalate containing layered double hydroxides, Opt. Mater. **80**, 186–196 (2018).

[24] N. Mahfoudh, K. Karoui, K. Khirouni, and A. Ben Rhaiem, Optical, electrical properties and conduction mechanism of $[(CH_3)_2NH_2]_2ZnCl_4$ compound, Physica B Condens. Matter **554**, 126–136 (2019).

[25] A. Laurikėnas, J. Barkauskas, J. Reklaitis, G. Niaura, D. Baltrūnas, and A. Kareiva, Formation peculiarities of iron (III) acetate: Potential precursor for iron and mixed-metal-organic frameworks (MOFs), Lith. J. Phys. **56**, 35–41 (2016).

[26] J.H. Yoon, S.B. Choi, Y.J. Oh, M.J. Seo, Y.H. Jhon, T.-B. Lee, D. Kim, S.H. Choi, and J. Kim, a porous mixed-valent iron MOF exhibiting the acs net: Synthesis, characterization and sorption behavior of $Fe_3O(F_4BDC)_3(H_2O)_3\cdot(DMF)_{3.5}$, Catal. Today **120**, 324–329 (2007).

[27] A. Abragam and B. Bleaney, *Electron Paramagnetic Resonance of Transition Ions* (Oxford University Press, Oxford, 2012).

[28] E. Coronado, C. Marti-Gastaldo, E. Navarro-Moratalla, and A. Ribera, Intercalation of $[M(ox)_3]^{3-}$ (M = Cr, Rh) complexes into (NiFeIII)-Fe-II-LDH, Appl. Clay Sci. **48**, 228–234 (2010).

[29] C.V. Popescu and E. Munck, Electronic structure of the H cluster in [Fe]-hydrogenases, J. Am. Chem. Soc. **121**, 7877–7884 (1999).

[30] N. Hoshino and T. Akutagawa, A trinuclear iron(III) complex of a triple noninnocent ligand for spin-structured molecular conductors, Chem. Eur. J. **24**, 19323–19331 (2018).

[31] J.F. De Conto, M.R. Oliveira, R.J. Oliveira, K.V. Campos, E.W. De Menezes, E.V. Benvenutti, E. Franceschi, C.C. Santana, and S.M. Egues, Synthesis of silica modified with 1-methylimidazolium chloride by sol-gel method: a comparison between microwave radiation-assisted and conventional methods, J. Non-Cryst. Solids **471**, 209–214 (2017).

[32] A.C. Sudik, A.P. Cote, and O.M. Yaghi, Metal-organic frameworks based on trigonal prismatic building blocks and the new 'acs' topology, Inorg. Chem. **44**, 2998–3000 (2005).

[33] J.M.D. Coey, *Magnetism and Magnetic Materials* (Cambridge University Press, Cambridge, New York, 2009).

[34] J.M.D. Coey, A. Barry, J. Brotto, H. Rakoto, S. Brennan, W.N. Mussel, A. Collomb, and D. Fruchart, Spin-flop in goethite, J. Phys. Condens. Matter **7**, 759–768 (1995).

[35] F. Bødker, M.F. Hansen, C.B. Koch, K. Lefmann, and S. Mørup, Magnetic properties of hematite nanoparticles, Phys. Rev. B **61**, 6826–6838 (2000).

[36] A. Vertes and D.L. Nagy, *Mössbauer Spectroscopy of Frozen Solutions* (Akadémiai Kiadó, Budapest, 1990).

[37] E. De Grave and R.E. Vandenberghe, ^{57}Fe Mössbauer effect study of well crystallized goethite (α-FeOOH), Hyperfine Interact. **28**, 643–646 (1986).

[38] C.A. Barrero, R.E. Vandenberghe, and E. De Grave, the effect of Al-content and crystallinity on the magnetic properties of goethites, Hyperfine Interact. **122**, 39–46 (1999).

[39] V. Klimas, K. Mažeika, V. Jasulaitienė, and A. Jagminas, Formation, morphology and composition of F- and Cl-stabilized iron β-oxyhydroxides, J. Fluor. Chem. **170**, 1–9 (2015).

[40] D. Chambaere and E. De Grave, On the Néel temperature of β-FeOOH: Structural dependence and its implications, J. Magn. Magn. Mater. **42**, 263–268 (1984).

[41] S.J. Oh, D.C. Cook, and H.E. Townsend, Characterization of iron oxides commonly formed as corrosion products on steel, Hyperfine Interact. **112**, 59–66 (1998).

[42] J. Marins, T. Montagnon, H. Ezzaier, C. Hurel, O. Sandre, D. Baltrūnas, K. Mažeika, A. Petrov, and P. Kuzhir, Colloidal stability of aqueous suspensions of polymer-coated iron oxide nanorods: Implications for biomedical applications, ACS Appl. Nano Mater. **1**, 6760–6772 (2018).

[43] P. Veverka, M. Pashchenko, L. Kubíčková, J. Kuličková, Z. Jirák, R. Havelek, K. Královec, J. Kohout, and O. Kamana, Rod-like particles of silica-coated maghemite: Synthesis via akaganeite, characterization and biological properties, J. Magn. Magn. Mater. **476**, 149–156 (2019).

[44] M. Catauro, F. Papale, and F. Bollino, Characterization and biological properties of TiO_2/PCL hybrid layers prepared via sol-gel dip coating for surface modification of titanium implants, J. Non-Cryst. Solids **415**, 9–15 (2015).

[45] C.P. Guntlin, S.T. Ochsenbein, M. Worle, R. Erni, K.V. Kravchyk, and M.V. Kovalenko, Popcorn-shaped Fe_xO (wustite) nanoparticles from a single-source precursor: Colloidal synthesis and magnetic properties, Chem. Mater. **30**, 1249–1256 (2018).

[46] A. Serra and E. Valles, Advanced electrochemical synthesis of multicomponent metallic nanorods and nanowires: Fundamentals and applications, Appl. Mater Today **12**, 207–234 (2018).

[47] V. Malik, A. Pal, O. Pravaz, J.J. Crassous, S. Granville, B. Grobety, A.M. Hirt, H. Dietsch, and P. Schurtenberger, Hybrid magnetic iron oxide nanoparticles with tunable field-directed self-assembly, Nanoscale **9**, 14405–14413 (2017).

[48] S. Tanaka, Y.V. Kaneti, R. Bhattacharjee, M.N. Islam, R. Nakahata, N. Abdullah, S.I. Yusa, N. Nam-Trung, M.J.A. Shiddiky, Y. Yamauchi, and M.S.A. Hossain, Mesoporous iron oxide synthesized using poly(styrene-*b*-acrylic acid-*b*-ethylene glycol) block copolymer micelles as templates for colorimetric and electrochemical detection of glucose, ACS Appl. Mater. Interfaces **10**, 1039–1049 (2018).

[49] H. Shokrollahi, Structure, synthetic methods, magnetic properties and biomedical applications of ferrofluids, Mater. Sci. Eng. C **33**, 2476–2487 (2013).

HIBRIDINIO ORGANINIO-NEORGANINIO $Fe_3O(TFBDC)_3(H_2O)_3\cdot(DMF)_3$ JUNGINIO SINTEZĖ LĖTO GARINIMO METODU. APIBŪDINIMAS IR MAGNETINIŲ SAVYBIŲ PALYGINIMAS

A. Laurikėnas [a], K. Mažeika [b], D. Baltrūnas [b], R. Skaudžius [a], A. Beganskienė [a], A. Kareiva [a]

[a] *Vilniaus universiteto Chemijos institutas, Vilnius, Lietuva*

[b] *Fizinių ir technologijos mokslų centras, Vilnius, Lietuva*

Santrauka

Lėto garinimo metodu susintetintas hibridinis organinis-neorganinis $Fe_3O(TFBDC)_3(H_2O)_3\cdot(DMF)_3$ junginys. Susintetintas naujas junginys buvo apibūdintas rentgeno spindulių difrakcinės (XRD) analizės, skenuojančios elektroninės mikroskopijos (SEM), energijos dispersinės rentgeno spindulių spektroskopijos (EDX) ir paramagnetinio rezonanso spektroskopijos (EPR) metodais. Susintetinto mėginio antiferomagnetinė / silpnai feromagnetinė reakcija buvo patvirtinta magnetėjimo ir Mössbauerio spektroskopijos tyrimų rezultatais. Susintetinta magnetinė medžiaga gali būti tiriama medicininiams tikslams ir panaudota kaip pirmtakas nanostruktūrinto geležies oksido sintezei.